Applied Catalysis B: Environmental 164 (2015) 251–260

Contents lists available at ScienceDirect

Applied Catalysis B: Environmental

journal homepage: www.elsevier.com/locate/apcatb

Fabrication of CeO_2/LDHs self-assemblies with enhanced photocatalytic performance: A case study on ZnSn-LDH matrix

E.M. Seftel[a,*], M.C. Puscasu[b], M. Mertens[c], P. Cool[a], G. Carja[b,**]

[a] Laboratory of Adsorption and Catalysis, Department of Chemistry, University of Antwerpen (CDE), Universiteitsplein 1, 2610 Wilrijk, Antwerpen, Belgium
[b] Department of Chemical Engineering, Faculty of Chemical Engineering and Environmental Protection, Technical University "Gh. Asachi" of Iasi, Bd. D. Mangeron, 700554 Iasi, Romania
[c] VITO Flemish Institute for Technological Research, Boeretang 200, B-2400, Belgium

ARTICLE INFO

Article history:
Received 5 June 2014
Received in revised form
10 September 2014
Accepted 16 September 2014
Available online 28 September 2014

Keywords:
Layered double hydroxides
Memory effect property
CeO_2
Phenol
Photocatalysis

ABSTRACT

The study reports the self-organization of CeO_2 nanoparticles on highly dispersed ZnO_6/SnO_6 octahedral units provided by a layered double hydroxide by a simple and environment friendly synthesis procedure. The obtained catalysts were thoroughly investigated by XRD, TG/DTG, chemical analysis, Raman and UV–vis DR spectroscopic techniques in order to obtain information on their crystalline structure and identity, CeO_2 content and photoresponsive properties. Furthermore, the controlled thermal treatment allowed us to obtain nano-coupled CeO_2/ZnO/SnO_2 systems with specific photocatalytic properties and their efficiency was tested for the phenol photodegradation under UV light. The data presented in this study shows that the phenol mineralization efficiency is strongly in relation with the presence of both the support and an optimum amount of CeO_2 organized on the layered matrix. This study highlights the positive effect of the combinations of the strategic cations like Zn–Sn or Ce–Zn–Sn in a nano-architectural assembly able to utilize the collective properties of the components for enabling their cumulative photocatalytic properties for "green" removal of dangerous pollutants.

1. Introduction

Removal pollutants from industrial process wastewaters have driven considerable research efforts as the amount and the quality of freshwater available in the world continues to decrease. Chemical and petroleum industries generate a wide variety of highly toxic organic wastes [1,2]. Among these, phenol and phenolic compounds, used as raw materials, have received increased attention due to their high toxicity. Phenol is known as human carcinogen and is of considerable health concern, even at low concentration [3,4]. Phenol can remain in air, soil, and water for long periods of time if a large amount of it is released at one time, or if it is constantly released in the environment from a source [3,5].

The treatment of industrial wastewaters for removal of the organic compounds is nowadays an important aspect of environmental technology. Technologies involving physical, biological or even chemical treatments do not achieve significant reduction of organic pollutants levels [4].

However, semiconductor photocatalysis may be considered as one of the most promising technology because it represents an easy way to utilize the energy of either natural sunlight or artificial indoor illumination, and thus abundantly available everywhere in the world [6].

Photocatalysis takes advantage of the high reactivity of the $HO^{\bullet}$ radicals in driving oxidation processes which are suitable for achieving complete mineralization of even most persistent and less reactive pollutants. It also requires the use of nanocrystalline semiconductors as photocatalysts, which initiate interfacial redox reactions [7,8].

TiO_2, ZnO and SnO_2 have been recognized to be preferable materials for photocatalytic processes due to their high photo-sensitivity, low cost and chemical stability [4,9–11]. ZnO nanostructures have been extensively investigated due to their interesting optical and electrical properties, and potential applications as UV light sources, sensors, photocatalysts, solar cells or piezoelectric devices [12,13]. SnO_2 is also regarded as of particular interest because it has outstanding optical, electrical and mechanical properties and is widely used as an attractive material for gas sensor applications, as a master element in optoelectronic

* Corresponding author. Tel.: +32 3 265 23 53; fax: +32 3 265 23 76.
** Corresponding author. Tel.: +40 232 278 680/2262; fax: +40 232 201 231.
E-mail addresses: seftel_elena@yahoo.com, elena.seftel@uantwerpen.be (E.M. Seftel), carja@uaic.ro (G. Carja).

http://dx.doi.org/10.1016/j.apcatb.2014.09.035
0926-3373/

devices or as a catalyst during oxidation of organic compounds [9,14].

The ZnO/SnO_2 system has been applied successfully as photocatalytic material demonstrating high photocatalytic efficiency than the single components [9,10,14]. The photoexcited electrons can be transferred between the conduction bands, e.g. from the ZnO side towards the SnO_2 side, and the holes between the valence bands, e.g. from the SnO_2 side to the ZnO side. As a consequence, the lifetime of the charge carriers is extended, and the charge separation is enhanced [9,10,15,16].

The most reactive rare earth oxide like ceria (CeO_2) may be also used for enhancing the catalytic oxidation of organic pollutants from wastewaters [17,18]. Cerium oxide has been employed as a photocatalyst in some of the reactions like water splitting, toluene oxidation and wastewater treatment [19,20]. CeO_2 exhibits a strong absorption in the UV range and its catalytic activity is mainly due to the redox couple Ce^{3+}/Ce^{4+} and the high capacity to store oxygen [21]. Moreover, the photogenerated electron–hole pairs are characterized by longer lifetimes than those generated by other photocatalysts, e.g. TiO_2 [18,22]. However, the use of pure CeO_2 always encounters disadvantages, the most important being the decrease of its oxygen storage capacity due to its rapid sintering under high temperatures [17]. Therefore, it is especially interesting to stabilize it on adequate supports which may offer the opportunity not only to improve its performance but also to form new stable compounds which lead to totally different physical and chemical properties from the individual components.

An interesting and suitable possibility is to construct a nanoarchitectonic based on nanosized cerium oxide and layered double hydroxide (LDHs) type materials. Layered double hydroxides are a class of naturally occurring anionic clays. Their structure arises from the isomorphous substitution of a divalent cation with a trivalent or tetravalent cation leading to the formation of positively charged brucite-like sheets held together by the anions located in the interlayer gallery, along with the crystallization water molecule [23]. They are represented by general formula $[M^{II}_{1-x}M^{III}_{x}(OH)_2]^{x+}A^{n-}_{x/n}\cdot mH_2O$, where the divalent M^{II} and trivalent M^{III} cations may be Mg^{2+}, Zn^{2+}, Ni^{2+}, Cu^{2+}, Al^{3+}, Fe^{3+}, Ti^{4+}, Sn^{4+}, etc., and the A^{n-} can be almost any organic or inorganic anion [23].

Our previous results demonstrated that the combination of ZnO/SnO_2 semiconductor mixed oxides generated from a ZnSn-LDH precursor showed much higher photocatalytic activity comparing with the corresponding physical mixtures [7]. It was found that the presence of Sn^{4+} in the layered double hydroxide-type precursor hinders the formation of the spinel-like phases which may reduce the photocatalytic performances.

Moreover, the advantages of using layered double hydroxides as a component of powerful photocatalysts with combined active sites are based on the following features: (i) the layered structures are composed of highly hydroxylated surfaces which was previously reported to enhance the photocatalytic activity [24,25], (ii) the versatility of the brucite-like sheets composition which may allow the insertion of strategic cations, like Zn^{2+} and Sn^{4+}, within the LDH network and thus might act as charge separation centers enhancing the efficiency in subsequent applications [7], (iii) can supply a good metal dispersion within the brucite-type layers, and as a consequence the formation of an intimate contact at atomic level between the generated semiconductor phases.

We previously studied the possibility to enhance the photocatalytic activity of CeO_2 nanoparticles by their assembly with ZnTi-containing layered matrix [26]. The obtained results indicated that the presence of the layered matrix induces a positive effect on the catalytic function of the obtained system. Moreover, by controlled thermal treatment, two types of photocatalytic nanocomposites are formed, e.g. ZnO/Zn_2TiO_4 starting from a ZnTi-LDH precursor, and CeO_2/Zn_2TiO_4 from a CeO_2 impregnated ZnTi-LDH precursor, respectively. When tested for phenol photodegradation in aqueous media, high catalytic efficiencies were observed, but depending on the photocatalytic system (ZnO/Zn_2TiO_4 or CeO_2/Zn_2TiO_4) different mineralization mechanisms were observed.

The present work reports CeO_2/ZnSn-LDHs and the derived mixed semiconductor oxides, $CeO_2/ZnO/SnO_2$, as novel photocatalytic materials for decomposition of phenol from wastewaters treatment under UV irradiation. The structural, phase transformation as a function of temperature and semiconducting properties of the studied catalysts are thoroughly investigated using XRD, TEM/SAED, TG/DTG, Raman and UV–vis DR spectroscopy techniques. Furthermore, the mechanism of phenol photodegradation by the studied photocatalysts is rationalized using UV–vis spectroscopy technique.

2. Experimental details

2.1. Synthesis of the ZnSn-LDH support

The layered double hydroxide support containing Zn^{2+} and Sn^{4+} with the cationic ratio of 3 was prepared by a co-precipitation method at constant pH with minor modification [7]. The ZnSn-LDH sample was prepared by the slow addition of a mixed $ZnCl_2$ and $SnCl_4\cdot 5H_2O$ solution (1 M in total, $Zn^{2+}/Sn^{4+} = 3$) to a Na_2CO_3 (2×10^{-3} M) solution under magnetic stirring. The co-precipitation agent was a diluted NaOH (0.1 M) solution. Previous research in the synthesis of ZnSn-LDH materials revealed that a zinc hydroxo stannate ($ZnSn(OH)_2$) phase is segregated along with the LDH material due to the excess amount of concentrated NaOH (2 M) solution [7]. Based on the detailed study on the formation mechanism previously described by Seftel et al. [7], during the synthesis the pH value was kept constant at 7 by the drop by drop addition of diluted NaOH (0.1 M) solution. The resulting slurry was aged about 12 h at room temperature. The final product was recuperated by filtration, washed several times with distilled water and dried at room temperature.

2.2. Synthesis of the CeO_2/ZnSn-LDH and the derived mixed oxide systems

1 g of the "freshly" calcined ZnSn-LDH (550 °C for 14 h) was added, under very vigorous stirring, at 250 ml of aqueous solutions of $Ce(SO_4)_2\cdot 4H_2O$ such that CeO_2 molar% vs. LDH would be 0.15–0.25. The final pH value of the reconstructed medium was approximately ~7. The obtained samples were aged at ambient temperature for 45 min, washed, centrifuged, dried under vacuum and denoted as n%CeO_2/ZnTiLDH. After calcinations at different temperatures up to 750 °C for 8 h the samples were denoted as n%CeO_2/ZnTi-T°C were, n stands for the loading percentage or CeO_2 nanoparticles and T for the calcination temperature.

2.3. Photocatalytic experiments

The photocatalytic activity of both ZnSn-LDH, n%CeO_2/ZnSn-LDH and the derived mixed oxides obtained by calcination at different temperatures was tested for the photodegradation of phenol in aqueous solution.

Appropriate amounts of a catalyst were dispersed into a phenol solution (50 mg/L) in a batch reactor at an optimal catalyst dose of 0.5 g/L. The temperature was kept constant at 25 °C, and the solutions were stirred in dark for 30 min in order to reach the adsorption–desorption equilibrium between the phenol molecules and the catalyst surface. Afterward, the solutions were irradiated

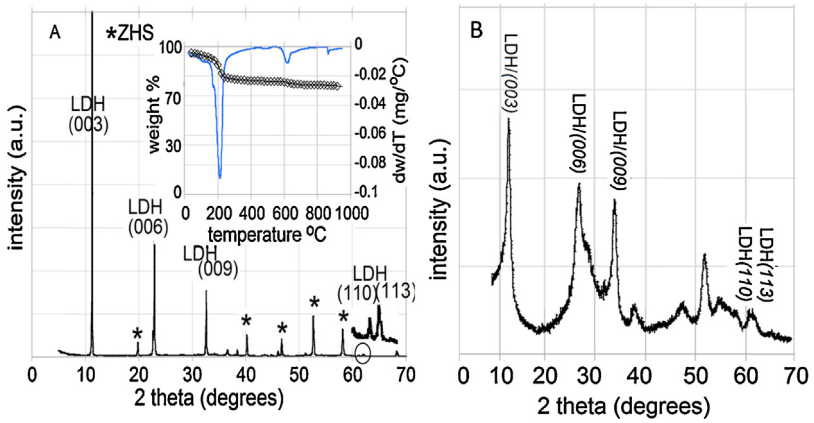

Fig. 1. The XRD pattern of A: ZnSn-LDH with TGA/DTG curves (inserted) and B: 0.15%CeO_2/ZnSn-LDH samples.

with UV-light up to 4 h by using a UV Pen-Ray Power Supply (UVP Products, TQ 718, 700 W) placed in a quartz tube, which was immersed in the solution. The phenol photodegradation profile was monitored by measuring UV–vis absorption spectra on a Jasco V550 spectrophotometer.

2.4. Characterization techniques

The structure and the crystal phases of the as synthesized solids were investigated by X-ray diffraction (XRD), transmission electron microscopy (TEM), FT-Raman, UV–vis diffuse reflectance spectroscopy (UV–vis-DR), and TG/DTA methods. The elemental analysis of the obtained solids was investigated by Electron Probe MicroAnalysis (EPMA) measurements.

X-ray diffractions were recorded on a PANalytical X'Pert PRO MPD diffractometer with filtered Cu Kα radiation; measurements were done in the 2θ mode using a bracket sample holder with a scanning speed of 0.04°/4 s in continuous mode. Transmission electron microscopy (TEM) images were performed on a Hitachi H99 trans-mission electron microscope operating at an accelerating voltage of 200 kV. Raman spectra were measured on a Nicolet Nexus 670 bench equipped with a Ge detector in a 180° reflective sampling configuration using a 1064 nm Nd:YAG laser. UV–vis-DR spectra were obtained at room temperature on a NICOLET EVOLUTION 500 UV–vis Spectrometer, with a diffuse reflectance accessory using KBr standard white as reflectance. Thermoanalytical measurements were performed on a Mettler Toledo TGA/SDTA851^e thermobalance. Samples were heated at a heating rate of 5 °C/min under O_2 flow.

3. Results and discussion

3.1. Structural characterization of the catalysts

Layered double hydroxide containing zinc and tin was prepared using the co-precipitation method at a constant pH. The material is composed of highly dispersed ZnO_6 and SnO_6 edge-sharing octahedrons within the brucite-like sheets of the LDHs [7,23]. Our previous results revealed that the controlled thermal treatment of this layered precursor leads to the formation of coupled ZnO/SnO_2 mixed semiconductor with higher photo-oxidative effect than the corresponding physical mixtures [7].

The LDHs type materials are characterized by the unique and remarkable *memory effect* property which consists in the spontaneous structural reconstruction of the original layered structure after being calcined and then placed in the vicinity of an aqueous solution containing anions. This behavior depends on several factors like the nature of the cations and their ratio within the brucite-like sheets, the nature of the anions used for the reconstruction as well as the calcination temperature on which the layered double oxide (LDO) is obtained [27–31].

Therefore, the formation of CeO_2/ZnSn-LDH self-assembly by taking advantage of the *memory effect* property was thoroughly investigated. This approach is a fast and facile route to obtain complex photocatalysts in mutual contact within atomic dimensions. Furthermore, calcination of CeO_2/ZnSn-LDH architecture gives rise to intimately dispersed nano-sized CeO_2/ZnO/SnO_2 mixed oxides having different band gap positions that can behave as semiconductors with remarkable photo-oxidative responses.

The XRD pattern of the parent ZnSn-LDH sample (Fig. 1A) reveals the formation of highly crystalline characteristic layered phase together with some minor portion of zinc hydroxo stannate (ZHS) phase. It is reported that when dealing with the incorporation of tetravalent cations within the LDHs lattice, a partial segregation of these cations as amorphous or crystalline phases on the surface of the brucite-like sheets occurs [32–34].

In the present study, the synthesis procedure was modified from our previous research [7] in order to decrease as much as possible the segregated ZHS phase, so we can take fully advantage of the *memory effect* property for further assembly with the CeO_2 nanoparticles. The unit cell parameters *c* and *a*, calculated from the characteristic (0 0 3) and (1 1 0) planes, of 2.28 and 0.31 nm, respectively. These values were compared with a conventional ZnAl-LDH material with the cationic ratio of 3 (c = 2.36 nm and a = 0.306 nm). The present obtained value for the *c* unit cell parameter indicates a decreased interlayer spacing due to increased electrostatic interaction with the interlayer species, induced by additional positive charges in the brucite-like sheets. Moreover, the increased cation–cation distance within the brucite-like sheets, reflected by the *a* unit cell parameter value, suggest that the obtained catalyst incorporated most of the Sn^{4+} cations within the LDH network forming the characteristic layered structure.

The crystallite sizes were calculated using the Scherrer equation [8] and the data are presented in Table 1.

The thermal stability and the phase transformation in temperature were studied using the TGA/DTG method (Fig. 1A, inserted picture). The DTG profile of ZnSn-LDH sample shows a weight loss at low temperatures (up to 100 °C) corresponding to the loss of the physically adsorbed water molecules on the external surface of the brucite-like sheets, followed by a major loss with the maximum at ~210 °C assigned to the decomposition of the carbonate anions and the dehydroxylation of the brucite-like sheets, as we previously reported for this type of materials [7]. Moreover, the small shoulder observed at 172 °C which may be assigned to the dehydroxylation of the ZHS phase [7,34]. As previously mentioned, the synthesis procedure was modified in order to incorporate most

Table 1
Phase composition and crystallite size observed for the obtained samples.

ZnSn-samples	Uncalcined	600 °C	750 °C
Phase[a]/crystallite size[b] (nm)	LDH/82.5 ZHS/57.7	ZnO/58 SnO_2/6.5	ZnO/58.8 SnO_2/11.4
0.15%CeO_2/ZnSn-samples[c]	Uncalcined	600 °C	750 °C
Phase[a]/crystallite size[b] (nm)	LDH/14.7 SnO_2/*nd* CeO_2/*nd*	ZnO/41.6 SnO_2/5.2 CeO_2/9.8	ZnO/36.7 SnO_2/9.8 CeO_2/31.2

[a] Based on the XRD and Raman observations.
[b] Calculated using the Scherrer equation [33] and selecting the (0 0 3) plane for the LDH phase; (1 0 0) plane for the ZnO phase; (1 1 1) plane for the CeO_2 phase; (3 1 1) plane for the Zn_2SnO_4 phase. nd—Not determined.
[c] 0.15 mol% of CeO_2 loading vs. LDH matrix calculated from Electron Probe Micro-Analysis (EPMA) results.

of the Sn^{4+} within the brucite-like sheets. The combination of the XRD and thermal analysis observations allows us to conclude that the segregation of the ZHS phase was overcome, as this is present as only a minor impurity on the obtained material. The TGA data indicates around 6 wt% but cannot give an exact value since the weight loss corresponding to the ZHS value is partially overlapped with the decomposition of the carbonate anions and the dehydroxylation step. On the other hand, a more exact value was obtained from the XRD data which indicated the presence of 6.4 wt% extra-framework ZHS phase. Another extra loss is observed in the range of 500–750 °C which can be associated with the conversion into a combined, highly dispersed ZnO/SnO_2 lattice.

When the freshly calcined ZnSn-LDH was introduced in the aqueous solution of cerium (IV) sulphate tetrahydrate the LDHs layered structure was recovered such that in the XRD pattern of 0.15%CeO_2/ZnSn-LDH (see Fig. 1B) the characteristic reflections corresponding to the (0 0 3), (0 0 6) and (0 0 9) planes and the non-basal reflections attributed to the (1 1 0) and (1 1 3) planes typical for the LDHs structure are identified. Due to the fact that very small NPs of CeO_2 reveal further structural differences induced by the reconstruction process the XRD patterns of the thermal treated ZnSn-LDH and 0.15%CeO_2/ZnSn-LDH are shown in Fig. 2. For ZnSn-LDH the controlled thermal treatment gives rise only to the mixed oxides: ZnO with a wurtzite-like structure and SnO_2 with rutile structure. On the other hand, the XRD pattern of the thermal treated CeO_2/ZnSn-LDH catalysts joins the characteristic reflections of CeO_2, ZnO and SnO_2 with different crystallite sizes depending on the calcination temperature as also indicated in Table 1. Characterization by transmission electron microscopy (TEM) technique further indicates that after the formation of small nanoparticles (NPs) organized on the bigger LDH particles (see Fig. 3). The presence of fine spherical rings/spots around the central bright region in SAED pattern discloses the existence of CeO_2 nanocrystallites distributed on the LDH matrix.

Further we used Raman technique to get more information about the reconstruction of the calcined ZnSnLDH in the solution of $Ce(SO_4)_2$ and the characteristics of CeO_2/ZnSn-LDH nano-assembly (Fig. 4). The parent ZnSn-LDH material (Fig. 4A, a) exhibits the characteristic vibration modes associated with the Zn-OH units (~550 cm^{-1}), Sn-OH units (268 cm^{-1}) and CO_3^{2-} anions within the interlayer gallery (1035 cm^{-1}) [32]. The Raman spectra of the reconstructed 0.15%CeO_2/ZnSn-LDH sample shows five vibration modes, with the maxima at 268, 464, 580, 985 and ~1070 cm^{-1}. The formation of very fine CeO_2NPs with a cubic fluorite structure is indicated by the presence of the F_{2g} vibration at 464 cm^{-1} [35]. The vibration modes observed at 260 and 550 cm^{-1} may be associated with the brucite-type lattice in the LDH phase, e.g. the cation-oxygen bonds of the M-OH units (M = Zn or Sn) [36,37]. The υ_1 vibration mode at 1035 cm^{-1} is now shifted to 985 cm^{-1} indicating the replacement of the CO_3^{2-} with SO_4^{2-} anions within the interlayer gallery. Accordingly, the vibration modes centered at 985, 1070 and 584 cm^{-1} may be correlated with the presence of the sulphate anions with a lowered symmetry in the interlayer gallery of the LDH phase. It was reported that the intense band at 985 cm^{-1} associated with the stretching (υ_1) vibration of the sulphate tetrahedral oxyanion and, in combination with the antisymmetric stretching (υ_3) vibration (splitted) may be regarded as a fingerprint of the LDH host matrix [36,38]. The splitting of the υ_3 mode indicates a significant symmetry lowering for the sulphate anions from T_d for the free anion to C_3 or C_{3v} for the intercalated anion within the LDH matrix [38]. These vibration modes are also observed for the 0.25%CeO_2/ZnSn-LDH sample (Fig. 4B, b), indicating the regeneration of the layered structure after the reconstruction step.

After the heat treatment at 600 °C, the narrowing of the F_{2g} vibration at 464 cm^{-1} may be correlated with the crystallization and growth of the nanosized CeO_2, which is in good agreement with the XRD observations. The vibrations previously observed for the Zn–OH and Sn–OH units are now of very low intensity revealing that the structure starts to collapse and changes into a solid solution with a good ordering of the cations. Moreover, the characteristic fingerprint for the sulphate anions may be still be observed as a low intensity band (Fig. 4A, c together with the inserted picture, and Fig. 4B, c, respectively) supporting the assumption the sulphate intercalated anions are offering a higher stability to the obtained LDH-type material. It is important to note that even after the calcination at 750 °C no other vibrations are detected which might suggest the formation of any type of spinel-like structure,

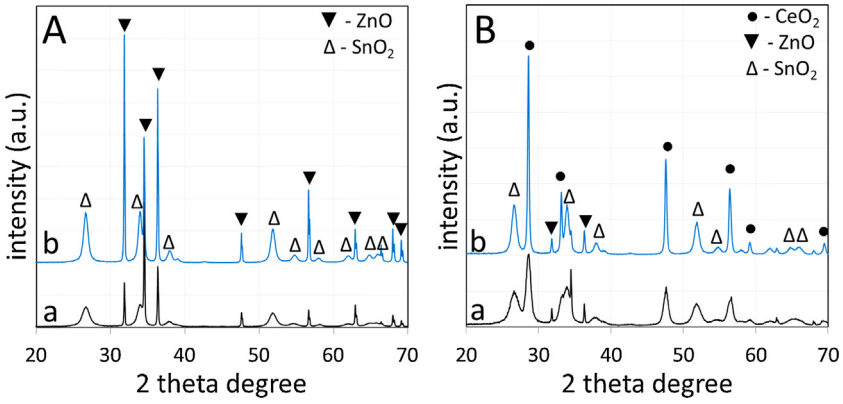

Fig. 2. The XRD patterns of A: (a) ZnSn-600 °C, (b) ZnSn-750 °C and B: (a) 0.15%CeO_2/ZnSn-600 °C, (b) 0.15%CeO_2/ZnSn-750 °C samples.

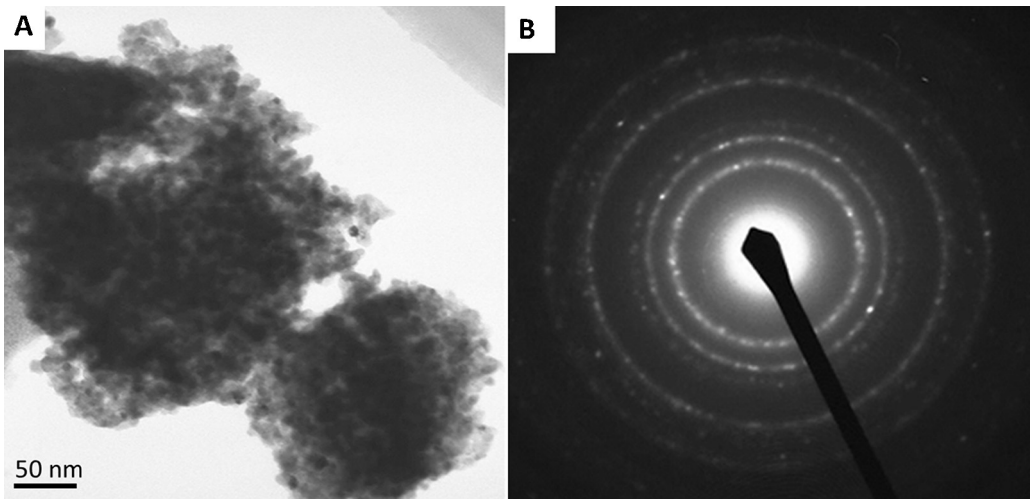

Fig. 3. Representative TEM image (A) and the corresponding SAED pattern (B) for the 0.15%CeO_2/ZnSn-LDH sample.

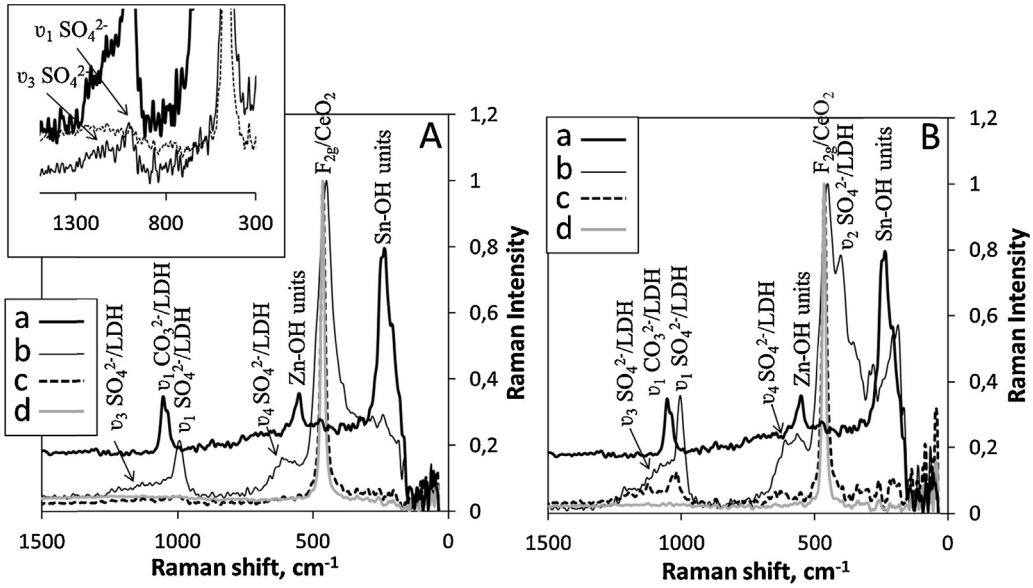

Fig. 4. Raman spectra of A: (a) ZnSn-LDH, (b) 0.15%CeO_2/ZnSn-LDH, (c) 0.15%CeO_2/ZnSn-600 °C and (d) 0.15%CeO_2/ZnSn-750 °C samples and B: (a) ZnSn-LDH, (b) 0.25%CeO_2/ZnSn-LDH, (c) 0.25%CeO_2/ZnSn-600 °C and (d) 0.25%CeO_2/ZnSn-750 °C samples. For clarity, the enlargement of the sulphate vibration region is presented in the inset picture.

e.g. $ZnSnO_3$ or Zn_2SnO_4, showing again that the heat treatment is not promoting the solid state reaction between the ZnO and SnO_2 phases. As it was previously reported the presence of the Sn^{4+} cations in the layered network hinders the formation of spinel-like phase in temperature [7,39]. Note that we also checked the phase composition by XRD and Raman measurements for samples calcined at 850 °C (results not shown), and no evidence of structural changings were observed. Therefore, more drastic conditions (e.g. higher temperatures and longer calcination times) are needed to promote the solid state reaction, indicating that the preservation of the metal dispersion in such a layered network is clearly an advantage for further applications. The υ_1 and υ_3 vibrations characteristic for the sulphate anions are no longer observed after calcination at 750 °C which may be well correlated with the formation of very fine and well crystallized mixed CeO_2/ZnO/SnO_2 lattice.

The UV–vis diffuse reflectance spectra of studied samples are shown in Fig. 5. This technique allowed us to investigate the cationic environment, phase composition when the samples are calcined at different temperatures and also to evaluate the band gap energies of the obtained coupled nano-sized photocatalytic systems.

For the parent ZnSn-LDH material, two regions may be distinguished from the UV–vis DR spectra. The Sn^{4+} cations may be identified in both ZHS [40] as well LDH [32] environment having an octahedral coordination. As also observed by XRD and Raman techniques, the calcination of the ZnSn-LDH sample at 600 °C changes the phase composition, the obtained material being composed of nanosized ZnO and SnO_2. These transformations are also observed by UV–vis DR technique, when changes of the absorption profiles with concomitant change in the energy band levels are observed. The UV–vis DR spectra of the ZnSn-600 °C shows the contribution of both phases by the appearance of a two-edge absorption profile as illustrated in Fig. 5A, b. The first absorption may be attributed to an indirect transition in the SnO_2 NPs, with the corresponding band gap energy of 3.0 eV. Further, the adsorption at higher wavelengths represents the contribution of the ZnO phase with a band gap energy of 3.1 eV. When the sample is further calcined

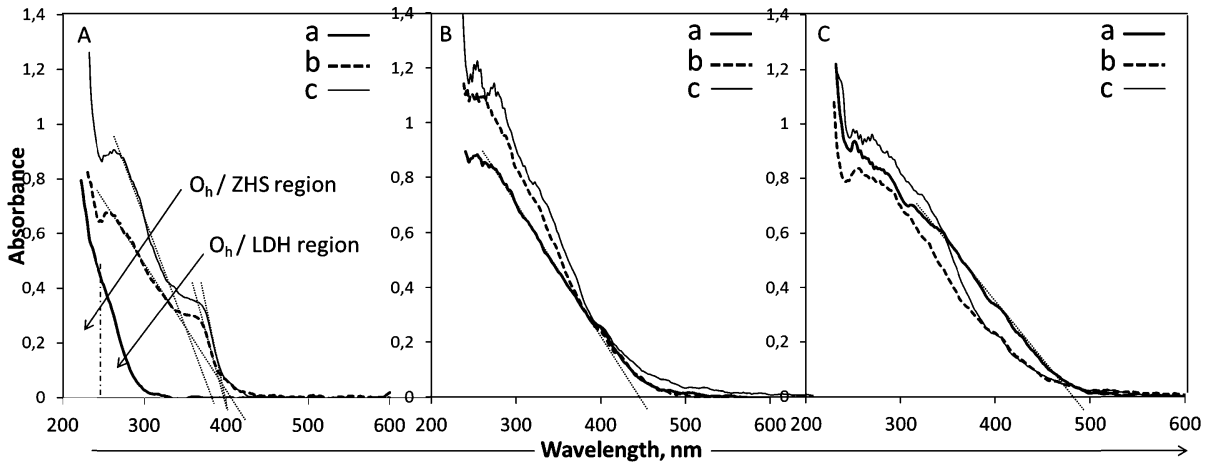

Fig. 5. The UV–vis diffuse reflectance spectra of A: (a) ZnSn-LDH, (b) ZnSn-600 °C, (c) ZnSn-750 °C; B: (a) 0.15%CeO_2/ZnSn-LDH, (b) 0.15%CeO_2/ZnSn-600 °C and (c) 0.15%CeO_2/ZnSn-750 °C and C: (a) 0.25%CeO_2/ZnSn-LDH, (b) 0.25%CeO_2/ZnSn-600 °C and (c) 0.25%CeO_2/ZnSn-750 °C samples.

up to 750 °C, the calculated values show an increase of the SnO_2 band gap energy to 3.2 eV and no modification of the ZnO band gap energy (3.1 eV), as it was previously reported for this type of coupled nano-sized ZnO/SnO_2 system [7,10].

The UV–vis DR spectra of the CeO_2 loaded ZnSn-LDH samples show different absorption profile indicating significant modification of the energy band levels. Firstly, the profile indicates the shift of the absorption to higher wavelengths which confirm the presence of the assembled components, e.g. the layered structure with Zn^{2+} and Sn^{4+} in octahedral environment and the presence of the cerium oxide nanoparticles. The absorption profile is now shifted about 80 nm towards visible range compared to ZnO (Fig. 5B, a), the entire system having a band gap energy of 2.8 eV. Further calcination at 600 and 750 °C leads to the slight increase of the band gap energy to 2.9 eV. These findings are very important for further application of the obtained nano-size coupled ZnO/SnO_2 and CeO_2/ZnO/SnO_2 systems as photocatalysts for the removal of organic pollutants. Hence, a good photocatalytic activity is expected for the obtained nano-assemblied systems.

3.2. Photocatalytic evaluation of the obtained nano-sized coupled systems

ZnSn-LDH, *n*%CeO_2/ZnSn-LDH samples as well as the derived nanoarchitectonics of the coupled mixed oxides were tested for the photodegradation of phenol under UV light. The photodegradation mechanism is strongly related to the reactive species involved in the phenol degradation process generated on the surface catalyst under UV irradiation. Moreover, as we previously reported [26], the photo-oxidative mineralization of phenol is described by a very complex mechanism. It involves first the formation of phenoxy radicals which, depending on the catalyst features, leads to different quinones followed by the opening of the aromatic ring, formation of the aliphatic acids, and finally mineralization to carbon dioxide and water [26,41].

The catalytic tests were realized at a catalyst dose of 0.5 g/L and UV–vis spectrophotometry was used to explain the evolution of the phenol photodegradation process. Our previous studies on the phenol decomposition process using the UV–vis spectrophotometry reveal that, even in the absence of phenol, the absorbance signal will be different from zero in the presence of any intermediary species resulting in the phenol photodegradation process. Therefore, for all the photocatalytic tests, the UV–vis absorption profile was recorded in the range between 190 and 400 nm in order to elucidate the photodegradation pathway involved for each studied catalytic system.

The kinetic of the photodegradation process in the presence of the ZnSn-LDH sample together with the absorption profile in different stage of reaction may be visualized in Fig. 6.

In the first stage of photocatalytic reaction, the mixtures of catalyst and phenol solution (25 mg/L) were stirred in dark conditions for approx. 30 min in order to establish the adsorption–desorption equilibrium between the phenol molecules and the catalyst surface. During this period, no significant modification in the absorption profile may be observed. When the UV radiation is turned on, differences in the absorption profiles are observed. For the ZnSn-LDH the absorption maximum in the region of 240 and 290 nm is decreased with a concomitant broadening of the absorption profile (Fig. 6d) due to a combined bathochromic and hypochromic effect indicating the beginning of the photodegradation process. This behavior might suggest the formation of the free radicals leading to catechol as an intermediary aromatic product, as this adsorbs in the same region broadening the absorption profile. Afterwards, increased time of irradiation leads to the opening of the aromatic ring and the formation of the aliphatic products may be observed as indicated by the absorption profile in the low wavelength region, e.g. 190–220 nm [42,43].

The photocatalytic degradation of phenol over the 0.15%CeO_2/ZnSn-LDH nanocomposite systems together with the UV–vis spectrum evolution as a function of irradiation time is shown in Fig. 7.

As it can be observed, the phenol photodegradation process occurs differently, and this can be associated with the presence of the CeO_2 nanoparticles on in the obtained nanocomposites.

No difference in the absorption profile is observed when the suspensions are stirred in dark (Fig. 6b). When the UV radiation is turned on, the aromatic ring is immediately opened and the muconic acid is formed, followed by its degradation to oxalic and formic acids and further to CO_2 and H_2O as final mineralization products. The direct formation of the muconic acid is indicated by the appearance of the hypsochromic effect broadening and shifting the absorption profile from 270 to 265 nm, indicating the formation of the muconic acid [43].

CeO_2 deposition on the surface of the layered network improves the mineralization efficiency for the obtained photocatalytic system as indicated by the data presented in Fig. 7a.

Therefore, the presence of the CeO_2 nanoparticles on the surface of the LDH material clearly changes the degradation pathway of phenol towards CO_2 and water. Even though the mineralization

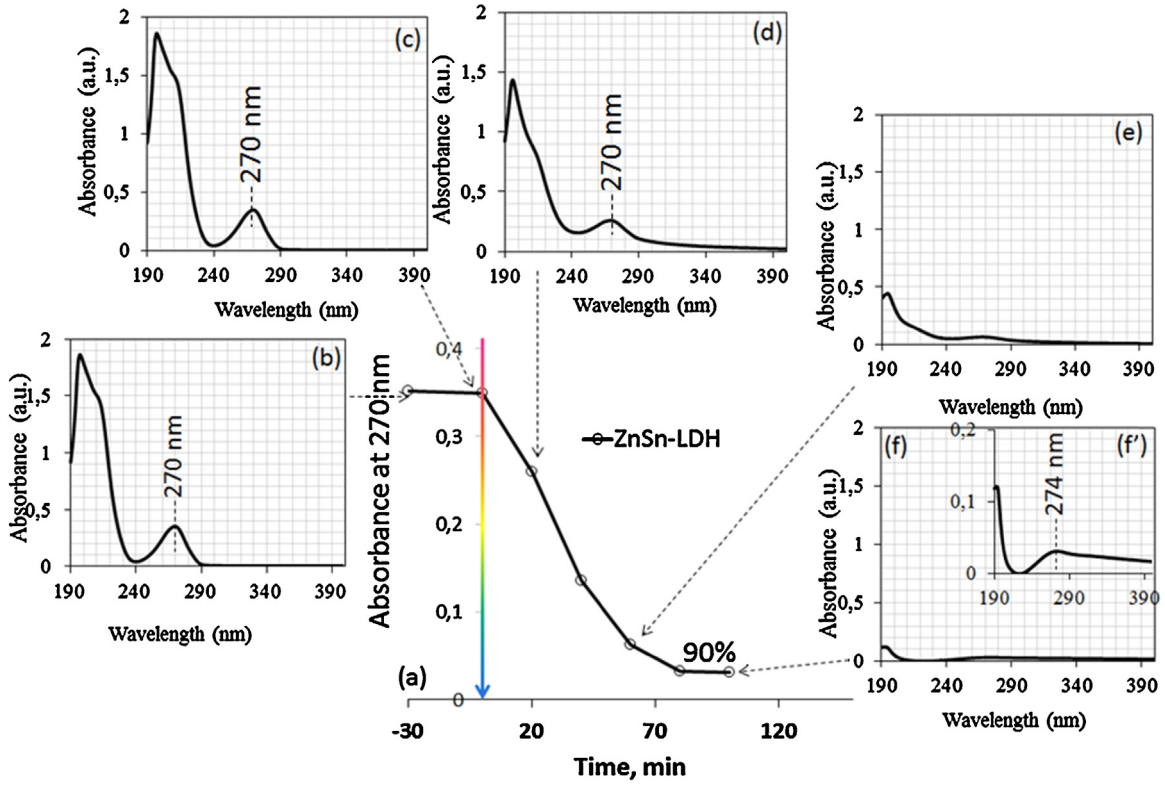

Fig. 6. Degradation kinetic (a) and UV–vis absorption profiles in different stages of phenol photodegradation process (b) initial phenol solution, (c) 30 min in dark, (d) 20 min UV, (e) 60 min UV and (f) and (f'-enlargement) 100 min in the presence of ZnSn-LDH sample.

degree is in the same range (90–92%) the presence of the CeO_2 nanoparticles leads to an immediate opening of the aromatic ring with the direct formation of the aliphatic intermediates, thus the reaction mixture becomes harmless from the toxicological point of view (correlated with the presence of aliphatic intermediates).

3.2.1. The influence of the CeO_2 Nps loadings in the studied nanoarchitectonics

The loading degree of catalytic active sites may strongly influence both the catalytic efficiency, as well as, the mineralization pathway of the phenol molecules. The influence of the loading amount of CeO_2 Nps (*n*%) in the studied nanoarchitectonics on the

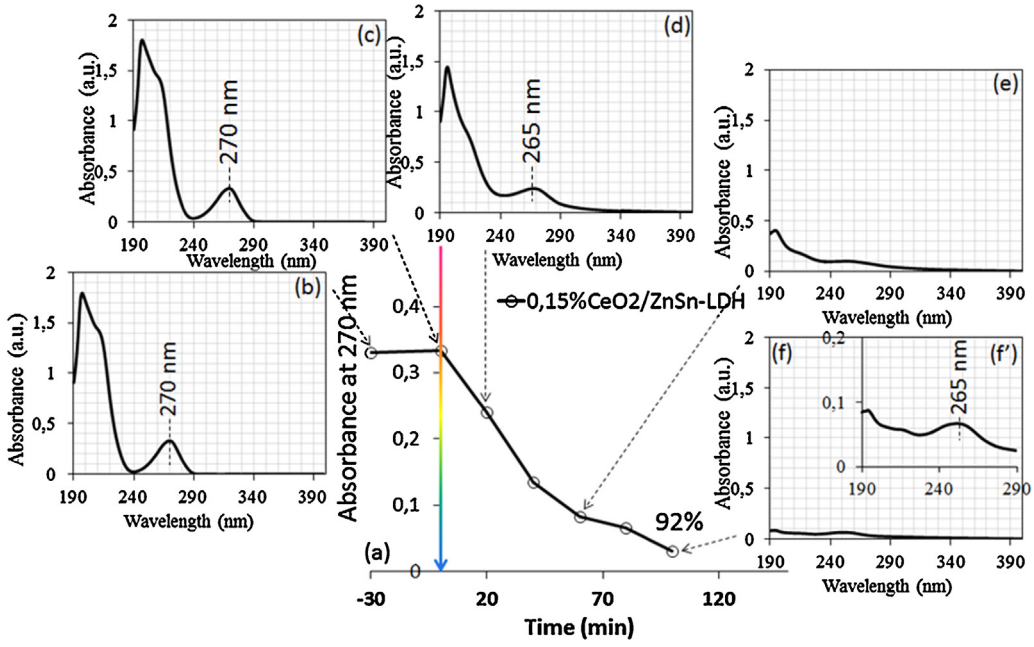

Fig. 7. Degradation kinetic (a) and UV–vis absorption profiles in different stages of phenol photodegradation process (b) initial phenol solution, (c) 30 min in dark, (d) 20 min UV, (e) 60 min UV and (f) and (f'-enlargement) 100 min in the presence of 0.15%CeO_2/ZnSn-LDH sample.

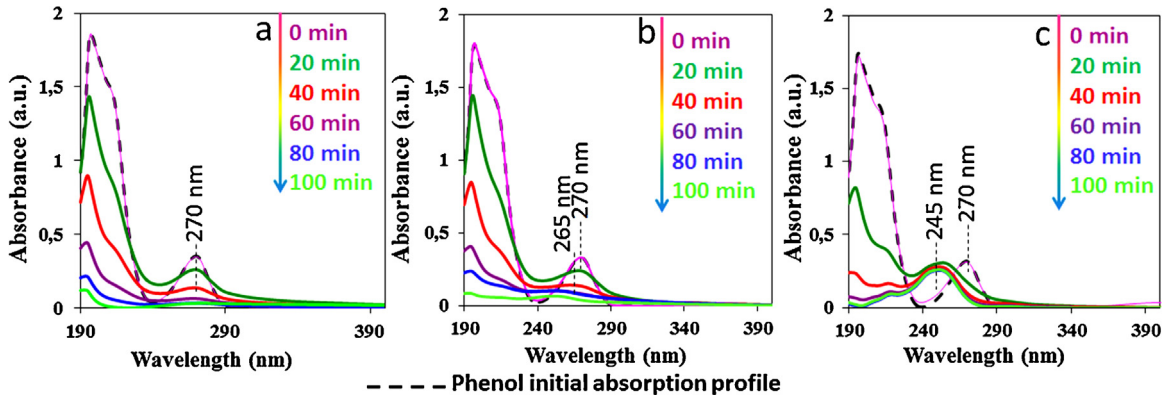

Fig. 8. Absorption spectra of phenolic solution during the photodegradation reactions using (a) ZnSn-LDH, (b) 0.15%CeO_2/ZnSn-LDH and (c) 0.25%CeO_2/ZnSn-LDH catalysts.

photocatalytic degradation pathway and efficiency is shown in Fig. 8.

It clearly shows that the presence and the amount of the CeO_2 NP on the surface of the LDH matrix gives rise to the different intermediary species when the samples are irradiated with UV light. This might suggest that this is an important factor to investigate since it directly influences the phenol degradation mechanism. The obtained results reveal that the phenol photodegradation occurs by two different mechanisms, e.g. ligand-to metal charge-transfer (LMCT) or UV-generated electron–holes pairs.

Thus, when the reaction mixture is stirred in dark, the adsorption–desorption equilibrium between the phenol molecules and the catalyst surface is established. For the ZnSn-LDH sample, when the UV light is turned on, a phenolate linkage is formed on the surface basic sites of the layered sheets which enables the light absorption through a ligand-to-metal charge transfer between the phenol (ligand) and the metal sites (Zn or Sn) of the ZnSn-LDH surface. It should be noted that the catalyst changed the color to light-brown immediately after the UV-light was turned on. This demonstrates the existence of the charge-transfer mechanism, as it was previously reported [22,44,45].

In the case of CeO_2 loaded samples, the 4*f* band plays an important role in the surface charge transfer reaction. Under UV illumination, an electron can be transferred from the ligand (phenol) to the catalyst and after this, to a suitable electron acceptor, such as O_2. Then, the radical species are formed which would be responsible of the hypsochromic effect observed in the UV–vis spectra of the phenolic solution in Fig. 8b and c. The experimental results show that the phenol photodegradation was considerably influenced by the CeO_2 content. The best performances were obtained for an optimal loading of 0.15 mol% vs. LDH matrix. This may be due to an enhanced interfacial charge transfer and improved the separation efficiency of the photogenerated electron–hole pairs, leading to an improved photocatalytic efficiency. When the CeO_2 content is higher than 0.15 mol%, the hypsochromic effect is remarkably enhanced indicating the excessive loading of CeO_2 nanoparticles decreasing the photocatalytic activity. Excessive loading may also block completely the surface hydroxyl groups which are certainly essential for the LMCT formation.

Accordingly, higher loadings of CeO_2 nanoparticles on the layered matrix showed a direct influence on the type of intermediates formed in the initial stage of photocatalytic reaction. 0.25 mol% vs. LDH matrix, leads immediately to the formation of *p*-benzoquinone as primary intermediate species (Fig. 8c), a very stable and toxic molecule. Only a very small part of this compound is degraded until the end of the photocatalytic test. These results may be explained taking into consideration that *p*-benzoquinone acts as $\bullet O_2^-$ radical scavenger and inhibits further the photo-oxidative effect [46], stabilizing the aromatic ring which is not opening further to form the corresponding aliphatic acids. Moreover, it indicates that in this case the LMCT does not occur and the photocatalysis takes places by the UV promoted electron from the valence band to the conduction band of the ceria nanoparticles followed by the formation of the oxidizing radical species (like $\bullet O_2^-$ and $HO\bullet$). The schematic representation of this mechanism may be visualized in Scheme 1. Therefore, the following photodegradation tests were realized using the 0.15%CeO_2/ZnSn-LDH samples.

3.2.2. *The influence of the calcination temperature*

The effect of the calcination temperature on both unloaded and CeO_2 loaded ZnSn-LDH samples is shown in Fig. 9. It can be seen that the photocatalytic activity in all cases decrease with the increased calcination temperature. This behavior can be associated with the phase transformation and growth of the crystallite size of the mixed oxides during calcination.

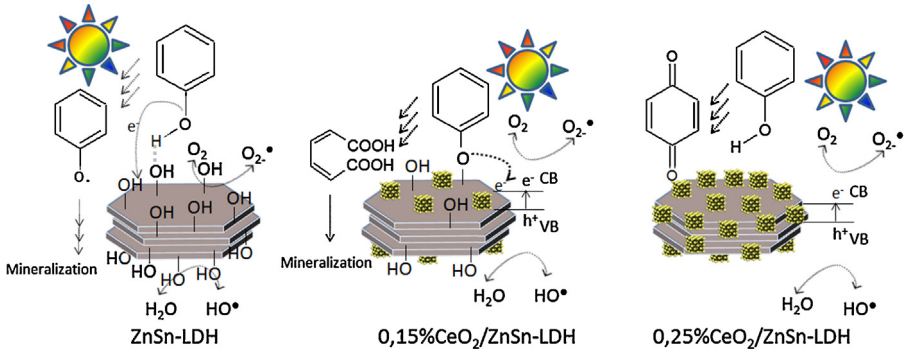

Scheme 1. Schematic representation of the photodegradation mechanism for the studied samples.

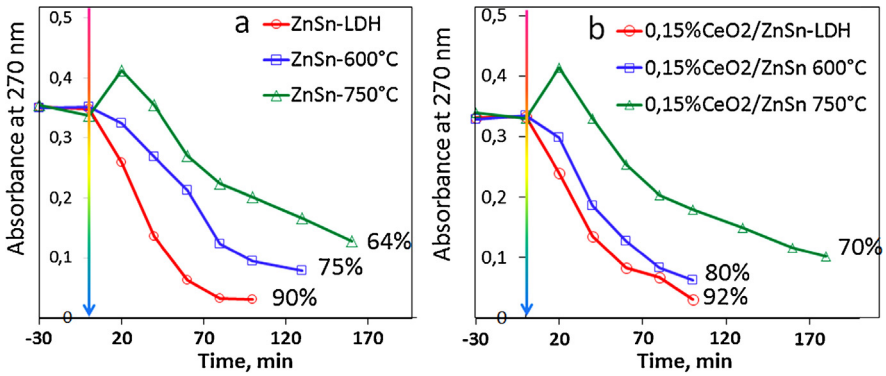

Fig. 9. Degradation of phenol under UV-light using (a) ZnSn-LDH and (b) 0.15%CeO_2/ZnSn-LDH samples.

As observed for both systems, the uncalcined samples showed stronger photo-oxidative effect that their corresponding mixed oxides. The decrease of the photocatalytic activity of the samples calcined at 600 °C may be associated with the dehydroxylation of the layered sheets. This behavior might suggest that the presence of highly hydroxylated surfaces in a layered network facilitates the formation of the •OH radicals which further ensures the sustainability of this photocatalytic process.

Further, it is also important to emphasize that the presence of the CeO_2 nanoparticles in the obtained catalysts leads to different intermediary species in the beginning of the photocatalytic tests, which affect the mineralization pathway as well as the efficiency of the entire process. As mentioned before, for the 0.15%CeO_2/ZnSn-LDH sample, after 20 min of irradiation, the aromatic ring is already opened and muconic acid is formed. For the uncalcined and 600 °C calcined catalysts samples, the concentration of the phenolic solution decreases immediately after turning on the UV lamp.

On the other hand, for the samples calcined at 750 °C, the absorption intensity increases after 20 min of irradiation. Accordingly, a mixture of catechol and resorcinol could be detected for the ZnSn-750 °C and 0.15%CeO_2/ZnSn-750 °C samples, as indicated by the combined bathochromic and hyperchromic effect leading to an increase of the absorbance in this region. The apparent concentration increases (Fig. 9, the green curves), but this can be associated with the formation of different chromophore groups and the formation of a mixture of catechol and resorcinol.

This behavior may be attributed to the difference in the phase composition as well as band gap positions characteristic for the different catalytic systems. Initially, the ZnSn-LDH sample consists of hydroxylated layered surfaces–surface basic sites, in which the highly dispersed ZnO_6 and SnO_6 octahedra are sharing edges forming the brucite-like characteristic network in the LDHs materials. The photocatalytic degradation of phenol is directly linked with the surface reactive species, e.g. HO•, $•O_2^-$, h_{VB}^+, e_{CB}^-. The results indicate that the photocatalytic efficiency is higher for the ZnSn-OH sample than for the ZnSn-600 °C and further, with the ZnSn-750 °C. The data suggest that the phenol degradation by oxidative pathway is the main degradation mechanism, hence that the highly hydroxylated ZnSn-LDH surface are enhancing the •OH radical formation. Therefore, up to 90%–92% of phenol was removed after 100 min of UV irradiation by the ZnSn-LDH and, 0.15%CeO_2/ZnSn-LDH samples.

Further on, the calcination up to 600 °C leads to changes into phase composition and the formation of intimately dispersed ZnO/SnO_2 and $CeO_2/ZnO/SnO_2$ semiconductor oxides was observed by XRD and UV–vis DR techniques (Figs. 2 and 5). Identical phenol photodegradation pathway is observed, with an efficiency of 75–80% in 130 min of reaction. Further calcination up to 750 °C leads to the increase of the crystallite size, and this has a direct effect on the photodegradation efficiency. Consequently, the formation of a mixed aromatic phase in the early stage of photocatalytic reaction was observed, and up to ~60–70% of phenol could be removed after longer time of reaction. The decrease in the photocatalytic activity can be correlated with the increased crystallite size in the generated coupled ZnO/SnO_2 and $CeO_2/ZnO/SnO_2$ systems, respectively.

The results show that the uncalcined samples are the most effective catalysts showing that the surface OH groups are an advantage for the photocatalytic process.

Comparing the photocatalytic systems described in this study, the best efficiency for the phenol photodegradation was observed for the 0.15%CeO_2/ZnSn-LDH and their calcined products, where the resulting degradation slurry contains no traces of *p*-benzoquinone, the mineralization products being CO_2 and water. Moreover, it is noteworthy that the presence of highly hydroxylated brucite-type sheets in the LDHs structure is an advantage for the photodegradation process.

Furthermore, the use of the LDH-type structure as preferred support for the deposition of metal oxide nanoparticles arises from the versatility of the brucite-like composition which may allow to introduce Zn^{2+} and Sn^{4+} within the network providing highly dispersed ZnO_6/SnO_6 units. The good dispersion of the metal cations within the layers may act as charge separation centers enhancing the efficiency in photocatalytic applications.

The results presented in this study demonstrate the positive effect of the combinations of the strategic cations like Zn-Sn or Ce-Zn-Sn in a catalyst with specific nanoarchitectonic able to utilize their collective properties enabling their cumulative photocatalytic properties for “green” removal of dangerous pollutants.

Moreover, this study highlights the influence of the nature of the cations within the brucite-like sheets of the LDH-type materials on the phase composition of the nanocomposites obtained by controlled thermal treatment of such precursors.

4. Conclusions

Novel efficient photocatalytic systems of CeO_2 nanoparticles loaded on layered double hydroxides were prepared by simple, fast and cheap route by taking advantage of the *memory effect* property of the LDH-type materials. The obtained photocatalysts were exposed to controlled thermal treatment to further obtain the nano-couples semiconductor $CeO_2/ZnO/SnO_2$ systems. The photocatalytic performances of the obtained catalysts were tested for the photodegradation of phenol in aqueous solutions. The phenol mineralization pathway was thoroughly investigated using the UV–vis spectroscopy technique. The experimental results indicated that the degradation of phenol is facilitated by the presence of the CeO_2 nanoparticles organized on the LDH matrix up to an optimal

loading. It was demonstrated that the use of the LDH-type structure provides several advantages when used as support for the deposition of metal oxide nanoparticles. The highly dispersed ZnO_6/SnO_6 units within the LDH network gives rise to a good dispersion of the metal cations within obtained materials. These may act as charge separation centers enhancing the efficiency in photocatalytic applications.

Acknowledgements

E.M. Seftel greatly acknowledges the Fund for Scientific Research—Flanders (FWO—Vlaanderen) for financial support. This work was also supported by the grant of the Romanian National Authority for Scientific Research, CNCS-UEFISCDI, Project number PN-II-ID-PCE-75/2013.

References

[1] L.F. Liotta, M. Gruttadauria, G. Di Carlo, G. Perrini, V. Librando, J. Hazard. Mater. 162 (2009) 588–606.
[2] M.C. Neves, J.M.F. Nogueira, T. Trindade, M.H. Mendonça, M.I. Pereira, O.C. Monteiro, J. Photochem. Photobiol. A: Chem. 204 (2009) 168–173.
[3] V.M. Brown, D.H.M. Jordan, B.A. Tiller, Water Res. 1 (1967) 587–594.
[4] J.C.K. Bubacz, D. Dolat, A.W. Morawski, Polish J. Environ. Stud. 19 (2010) 685–691.
[5] N. Belhadj Tahar, A. Savall, Electrochim. Acta 54 (2009) 4809–4816.
[6] H. Tong, S. Ouyang, Y. Bi, N. Umezawa, M. Oshikiri, J. Ye, Adv. Mater. 24 (2012) 229–251.
[7] E.M. Seftel, E. Popovici, M. Mertens, E.A. Stefaniak, R. Van Grieken, P. Cool, E.F. Vansant, Appl. Catal. B: Environ. 84 (2008) 699–705.
[8] E.M. Seftel, E. Popovici, M. Mertens, K.D. Witte, G.V. Tendeloo, P. Cool, E.F. Vansant, Micropor. Mesopor. Mater. 113 (2008) 296–304.
[9] A. Hamrouni, H. Lachheb, A. Houas, Mater. Sci. Eng.: B 20 (2013) 1371–1379.
[10] C. Wang, X. Wang, B.-Q. Xu, J. Zhao, B. Mai, A.P. Peng, G. Sheng, J. Fu, J. Photochem. Photobiol. A: Chem. 168 (2004) 47–52.
[11] C. Wang, B.-Q. Xu, X. Wang, J. Zhao, J. Solid State Chem. 178 (2005) 3500–3506.
[12] J. Xie, H. Wang, M. Duan, L. Zhang, Appl. Surf. Sci. 257 (2011) 6358–6363.
[13] H.J. Fan, Y. Yang, M. Zacharias, J. Mater. Chem. 19 (2009) 885–900.
[14] M.M. Rashad, A.A. Ismail, I. Osama, I.A. Ibrahim, A.-H.T. Kandil, Arab. J. Chem. 7 (2014) 71–77.
[15] W. Cun, Z. Jincai, W. Xinming, M. Bixian, S. Guoying, P. Ping'an, F. Jiamo, Appl. Catal. B: Environ. 39 (2002) 269–279.
[16] Y.-J. Chiang, C.-C. Lin, Powder Technol. 246 (2013) 137–143.
[17] J. Fang, X. Bi, D. Si, Z. Jiang, W. Huang, Appl. Surf. Sci. 253 (2007) 8952–8961.
[18] A. Corma, P. Atienzar, H. Garcia, J.-Y. Chane-Ching, Nat. Mater. 3 (2004) 394–397.
[19] B. Jiang, S. Zhang, X. Guo, B. Jin, Y. Tian, Appl. Surf. Sci. 255 (2009) 5975–5978.
[20] M.L. Dos Santos, R.C. Lima, C.S. Riccardi, R.L. Tranquilin, P.R. Bueno, J.A. Varela, E. Longo, Mater. Lett. 62 (2008) 4509–4511.
[21] T. López, F. Rojas, R. Alexander-Katz, F. Galindo, A. Balankin, A. Buljan, J. Solid State Chem. 177 (2004) 1873–1885.
[22] J.S. Valente, F. Tzompantzi, J. Prince, Appl. Catal. B: Environ. 102 (2011) 276–285.
[23] F. Cavani, F. Trifirò, A. Vaccari, Catal. Today 11 (1991) 173–301.
[24] E.M. Seftel, M. Mertens, P. Cool, Appl. Catal. B: Environ. 134–135 (2013) 274–285.
[25] E.M. Seftel, E. Popovici, E. Beyers, M. Mertens, H.Y. Zhu, E.F. Vansant, P. Cool, J. Nanosci. Nanotechnol. 10 (2010) 8227–8233.
[26] E.M. Seftel, M.C. Puscasu, M. Mertens, P. Cool, G. Carja, Appl. Catal. B: Environ. 150–151 (2014) 157–166.
[27] N. Das, A. Samal, Micropor. Mesopor. Mater. 72 (2004) 219–225.
[28] A.E. Palomares, J.G. Prato, F. Rey, A. Corma, J. Catal. 221 (2004) 62–66.
[29] G. Carja, L. Dartu, K. Okada, E. Fortunato, Chem. Eng. J. 222 (2013) 60–66.
[30] G. Carja, E. Husanu, C. Gherasim, H. Iovu, Appl. Catal. B: Environ. 107 (2011) 253–259.
[31] G. Carja, G. Lehutu, L. Dartu, M. Mertens, P. Cool, Appl. Clay Sci. 65–66 (2012) 37–42.
[32] E.P.E.M. Seftel, M. Mertens, P. Cool, E.F. Vansant, J. Optoelectron. Adv. Mater. 10 (2008) 3477–3481.
[33] E.M. Seftel, E. Popovici, M. Mertens, G. Van Tendeloo, P. Cool, E.F. Vansant, Micropor. Mesopor. Mater. 111 (2008) 12–17.
[34] S. Velu, K. Suzuki, T. Osaki, F. Ohashi, S. Tomura, Mater. Res. Bull. 34 (1999) 1707–1717.
[35] Q.-H. Xu, D.-M. Xu, M.-Y. Guan, Y. Guo, Q. Qi, G.-D. Li, Sensors Actuators B: Chem. 177 (2013) 1134–1141.
[36] F.F.C. Ardau, P.C. Ricci, C. Cannas, E. Dore, P. Lattanzi, Mine Water—Manag. Challenges (2011) 559–562.
[37] P. Mendes, M. Moreira, S. Tebcherani, M. Orlandi, J. Andrés, M. Li, N. Diaz-Mora, J. Varela, E. Longo, J. Nanopart. Res. 14 (2012) 1–13.
[38] R.L. Frost, A.W. Musumeci, W.N. Martens, M.O. Adebajo, J. Bouzaid, J. Raman Spectrosc. 36 (2005) 925–931.
[39] M. Intissar, F. Malherbe, V. Prévot, F. Leroux, J. Colloid Interface Sci. 299 (2006) 747–753.
[40] H. Li, W. Hong, Y. Cui, Q. Jia, S. Fan, J. Mol. Catal. A: Chem. 378 (2013) 164–173.
[41] C. Borras, C. Berzoy, J. Mostany, J.C. Herrera, B.R. Scharifker, Appl. Catal. B: Environ. 72 (2007) 98–104.
[42] C.E. Lund Myhre, C.J. Nielsen, Atmos. Chem. Phys. 4 (2004) 1759–1769.
[43] P.E.G.L.H.J.M. Carreira, M. Graca, V.S. Carvalho, D.V. Evtuguin, Tappi J. 11 (2012) 59–67.
[44] T.-X. Liu, X.-Z. Li, F.-B. Li, Chem. Eng. J. 157 (2010) 475–482.
[45] Y.S. Seo, C. Lee, K.H. Lee, K.B. Yoon, Angew. Chem. Int. Ed. 44 (2005) 910–913.
[46] L. Mohapatra, K.M. Parida, Sep. Purif. Technol. 91 (2012) 73–80.